VOLUME 7, NUMBER 8, AUGUST 2007

NANO LETTERS

Selective Vibrational Detachment of Microspheres Using Optically Excited In-Plane Motion of Nanomechanical Beams

B. Ilic,*,† S. Krylov,‡ M. Kondratovich,§ and H. G. Craighead†

School of Applied and Engineering Physics, Nanobiotechnology Center and Cornell Nanofabrication Facility, Cornell University, 250 Duffield Hall, Ithaca, New York 14853, School of Mechanical Engineering, Tel Aviv University 69978 Ramat Aviv, Israel, and School of Mechanical and Aerospace Engineering and Cornell Nanoscale Facility, Cornell University, 250 Duffield Hall, Ithaca, New York 14853

Received September 18, 2006; Revised Manuscript Received June 11, 2007

ABSTRACT

Optical excitation plays an important role in the actuation of higher flexural and torsional modes of nanoelectromechanical oscillators. We show that optical fields are efficient for excitation, direct control, and measurement of in-plane motion of cantilever-type nanomechanical oscillators. As a model system, 200- and 250-nm-thick single-crystal silicon cantilevers with dissimilar lengths and widths ranging from 6 to 12 μm and 500 nm to 1 μm, respectively, were fabricated using surface micromachining and dynamically analyzed using optical excitation and interferrometric detection. Three-dimensional finite element analysis incorporating shear, rotational inertia, cross-sectional deplanation, and nonideal boundary conditions due to the structural undercut describe the dynamics of the nanomechanical structures adequately. The quality factor of a particular in-plane harmonic was consistently higher than the transverse mode. The increased dissipation of the out-of-plane mode was attributed to material and acoustic loss mechanisms. The in-plane mode was used to demonstrate vibrational detachment of submicrometer polystyrene spheres on the oscillator surface. In contrast, the out-of-plane motion, even in the strong nonlinear impact regime, was insufficient for the removal of bound polystyrene spheres. Our results suggest that optical excitation of in-plane mechanical modes provide a unique mechanism for controlled removal of particles bound on the surface of nanomechanical oscillators.

Manipulating the dynamics of flexural and torsional vibrational modes of micro-[1−9] and nanoelectromechanical systems[10−22] (MEMS and NEMS) with external fields has long been a sought-after goal. A widely studied class of NEMS devices consists of surface micromachined mechanical oscillators made of thin-film layers patterned into various shapes that operate by motion perpendicular to the plane of the thin film and substrate by bending in their thin direction. Conventional mechanical driving and motion transduction

* Corresponding author. E-mail: bi22@cornell.edu.
† School of Applied and Engineering Physics, Nanobiotechnology Center and Cornell Nanofabrication Facility, Cornell University.
‡ Tel Aviv University.
§ School of Mechanical and Aerospace Engineering and Cornell Nanoscale Facility, Cornell University.

10.1021/nl0621950 CCC: $37.00
Published on Web 07/14/2007

methods typically activate and detect motion only in this out-of-plane, transverse direction.[10,23,24] Previously, we demonstrated a robust method for driving and detecting the motion of micro- and nanoscale resonators by utilizing the optical drive of resonant motion and interferometric detection of that motion by a separate laser.[25,26] This technique allowed noninvasive activation and interrogation of individual oscillators or arrays of oscillators.[27] Here we describe an approach that can activate and detect the perpendicular, in-plane motion of such oscillators. Because the frequency ranges and mechanical loss mechanisms can vary for the motion in the two directions, access to the different modes of oscillation can be useful in exploring anisotropic material properties or utilizing alternate directions of motion in device applications. In our case, we are interested in the applications of arrays of oscillators as sensors and for binding force measurements. We also wish to study selective binding and sorting of nanoscale objects based on mass or surface adhesion properties. Toward this end, we have demonstrated the controlled capture, detection, and release of submicrometer particles by the application of forces imparted by the in-plane motion of the resonators. To our knowledge, this work represents the first experimental demonstration of optical drive and detection of in-plane motion.

In this work, vibrational excitation and motion detection were accomplished using an optical setup comprised of an amplitude-modulated 415-nm diode laser in conjunction with a HeNe interferrometric reflectance system. We observed the first and second in-plane vibrational modes for slender cantilevers with lengths exceeding 8.5 μm. Because of the high deformations at the clamped edge arising from the undercut of the sacrificial silicon dioxide (SiO_2) layer, measured higher order out-of-plane, transverse modes showed deviation from the ideally clamped Euler−Bernoulli beam calculations. A full three-dimensional finite element analysis, considering dimensions of the cantilever derived from scanning electron microscopy, enabled us to identify various observed flexural and torsional vibrational modes. Higher-order out-of-plane vibrations and energy dissipation were affected considerably by the silicon overhang resulting from the sacrificial SiO_2 removal. In contrast, these nonideal boundary conditions are less-influential on the dynamics of in-plane vibrational modes. The in-plane, as well as torsional, modes of vibration were not observed when the single-crystal silicon devices were driven using a piezoelectric actuator. The consequences are perhaps due primarily to the inefficient energy coupling between the piezo and the substrate. As a model system, we have employed in-plane oscillations to remove weakly bound polystyrene spheres from the oscillator surface. In contrast, transverse oscillations were insufficient for the removal of the spherical beads.

Our cantilevers were fabricated from commercially available silicon-on-insulator (SOI) (100) wafers (SOITEC). The top structural silicon layer was 200- and 250-nm-thick with a measured uniformity of less than 2%. Devices of varying lengths ($l = 6-12$ μm) and widths ($w = 500$ nm-1 μm) were defined using optical projection lithography and etched with a CF_4 plasma. The exposed 1-μm-thick sacrificial SiO_2 layer was removed using 49% hydrofluoric acid. Dynamic properties of the cantilevers were calculated and modeled for the geometry determined from optical and scanning electron microscopy. Rounding of the corners at the clamped and free end, due to optical proximity effects during lithographic definition of the beam, along with the undercut was incorporated into the three-dimensional finite element model.

The released oscillators were then placed into a chamber that was evacuated to a pressure of 2×10^{-7} Torr. A custom-built optical setup with two laser beams was used to excite and detect the oscillatory motion of the cantilever.[26] Reflectance variations from the incident He−Ne laser focused at the free end of the cantilever beam were measured using a single-cell photodetector. A spectrum analyzer was used to collect the output signal from the photodetector and apply the excitation to the electrooptic modulator (EOM) controlling the 415-nm diode laser used to actuate the oscillator. The energy of the incident light couples directly into the device layer through localized temperature variations. The local temperature change from the absorbed laser beam creates stresses that couple mechanical energy to the oscillator. The transverse motion of the cantilever was measured interferrometrically from reflectance variations caused by the Fabry−Perot cavity formed by the oscillating beam and the silicon substrate.[10] At resonance, the in-plane vibrations, however, act as a mechanical optical chopper. In this scenario, the reflected He−Ne laser is partially interrupted causing dynamic changes in the area of the Fabry−Perot cavity. The reflected light intensity variations impinging on the single-cell photodetector reveal the NEMS vibrations (Figure 1a). The frequency of oscillation and the mechanical quality factors were determined by fitting the frequency spectra to Lorentzian functions. Specific vibrational modes were excited by sweeping the excitation frequency over a wide spectral range. Various observed resonances, corresponding to different modes of vibration, were identified and compared to values predicted by the model. Our calculations show that for a few of the lowest modes, the discrepancy between the calculated and measured values, as well as scattering in measured results, is smaller than the difference between frequencies corresponding to various vibrational modes.

To identify the type of vibrational mode, the eigenfrequencies of the cantilever were first calculated and the corresponding eigenmodes were built using beam theory. For a linearly elastic, homogeneous, and isotropic material, the eigenfrequencies of transverse and in-plane flexural vibrations of a prismatic cantilever beam described in the framework of the Euler−Bernoulli theory are calculated using the following expressions[28]

$$f_{o\xi} = \frac{\beta_\xi^2}{2\pi}\left(\frac{t}{l^2}\right)\left(\frac{E}{12\rho}\right)^{1/2} \quad (1)$$

and

$$f_{i\,\xi} = \frac{\beta_\xi^2}{2\pi}\left(\frac{w}{l^2}\right)\left(\frac{E}{12\rho}\right)^{1/2} \quad (2)$$

where β_ξ is the frequency parameter, ξ is the mode number, E is the Young's modulus, ρ is the mass density, and the

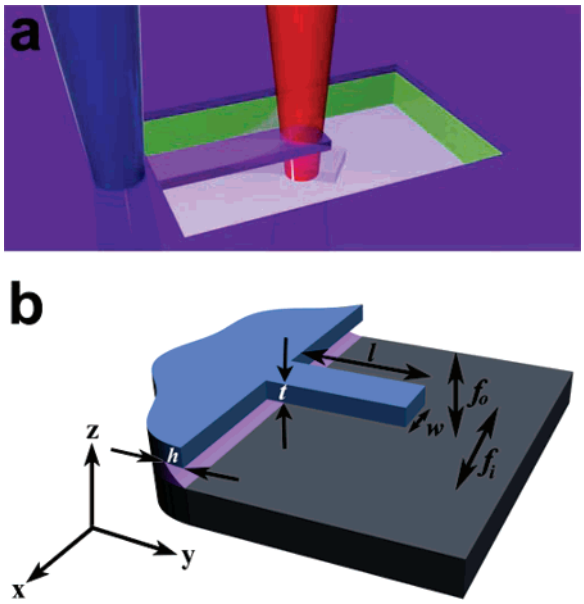

Figure 1. (a) Schematic illustration of the optical actuation and detection setup. Single-crystal Si cantilever devices were separated from the underlying Si substrate by a 1-μm-thick SiO_2 layer. The driving signal generated by the 415-nm blue diode laser is focused in close proximity to the clamped end of the beam. In-plane motion of the oscillator generates a chopping response, causing intensity variations of the reflected interferrometric He−Ne laser beam. (b) Sketch of the rectangular cantilever configuration. Typical cantilever dimensions range from $w = 0.5-1$ μm, $l = 6-12$ μm, and $t = 200-250$ nm. The extent of the device layer overhang was $h = 1$ μm. Arrows indicate transverse out-of-plane and in-plane motion with the frequencies f_o and f_i, respectively.

cantilever dimensions (w, l, t) are shown in Figure 1b. The ratio of the two oscillatory modes yields a dimensionless quantity $\Phi = w/t$. For the fabricated devices of 1-μm width and 200-nm thickness, $f_{i\zeta} = 5\, f_{o\zeta}$. The values of the Young's modulus, Poisson's ratio, and mass density of the single-crystal Si adopted in our calculations were $E = 169$ MPa, $\nu = 0.28$, and $\rho = 2300$ kg/m^3, respectively.

For the devices with dimensions $l = 6.6$ μm, $w = 1$ μm, and $t = 200$ nm, the first eigenfrequencies for the transverse and in-plane modes are shown in Figure 2a and b, respectively. The measured ratio between the two modes $\Phi_{\text{measured}} \sim 5.12$ was in good agreement with the Euler−Bernoulli theory ($\Phi = 5$). With this oscillator length, second (Figure 2c) and third (Figure 2d) transverse harmonics were also measured; however, higher in-plane vibrational modes were not detected. Additionally, excitations above the third out-of-plane harmonic were not observed. This is attributed to the dramatic contrast of the compliance between the two modes. Neglecting rounding of the corners at the clamped and free end, the calculated compliance for the transverse and in-plane directions was $c_o = 0.855$ m/N and $c_i = 0.043$ m/N respectively. However, with fabricated devices of lengths exceeding 8.5 μm, we measured up to the second in-plane mode.

The measured frequency ratio between the two modes for the first and second harmonics for a $l = 8.5$ μm beam were $f_{i1}/f_{o1} = 5.06$ and $f_{i\,2}/f_{o2} = 4.97$, respectively. This is in excellent agreement with the theoretically predicted value of 5. Higher flexural as well as torsional modes were observed with the $l \geq 8.5$ μm cantilevers.

In addition to the Euler−Bernoulli (EB) theory, the eigenfrequenceis and eigenmodes of the beam were obtained using the three-dimensional finite element (FE) simulations. The model was built using a commercially available package ADINA and accounts for the influence of geometric and clamping imperfections, mainly cantilever edge rounding and the overhang at the clamped end of the beam. Three-dimensional 27-node solid elements with quadratic interpolating functions in each direction were used to mesh the beam and the overhang. The results provided by the various models, summarized in Table 1, collectively allow identification of the type of vibrational response measured in our experiments.

Three-dimensional FE analysis showed that the nonideal clamping conditions caused by the overhang[8,29] reduce the eigenfrequencies of the cantilever significantly. The influence of the semiflexible clamping overhang region on the transverse vibrational modes, especially higher modes, were more pronounced while its effect on the in-plane vibrations was minor. The insets of Figure 2 illustrate the modal stress field amplitude along the surface of the cantilever. The figure also shows the localized character of the stress intensity maxima at the nodal points of the mode. Moreover, the analysis of the stress induced by the transverse vibrations shows the stress field propagation and the deformation of the overhang region. For example, a 6.6-μm-long beam with a 1-μm-deep undercut led to a decrease of the first transverse harmonic by 14.5%. In contrast, the in-plane resonant frequency decreased by 8.8% (see Table 1). This result implies that the in-plane vibrations are less-sensitive to the overhang. The lack of penetration of the stress fields beyond the clamped end (see the inset of Figure 2b) further supports the conclusion that the flexible overhang has limited influence on the vibrational character of the in-plane modes. Furthermore, our modeling results show that nonideal, rounded corners of the cantilever at the clamped and free ends result in an increase of the predicted modal frequency values. This effect is more notable for the in-plane vibrations.

Having established the distinction between various vibrational modes, in the following treatment, as a model system, evaluation of employing in-plane oscillations to remove weakly bound polystyrene spheres was considered. First, submicrometer polystyrene spheres suspended in water were allowed to dry slowly in air. When suspended in water, polystyrene spheres acquire negative charge on their surfaces.[30] The dry polystyrene spheres with diameters ranging from 500 nm to 1 μm diameter were then randomly interspersed onto the surface of a 1-cm^2 chip containing a periodic array of a large number ($>10^6$) of NEMS resonators. Figure 3a shows random scattering of weakly bound polystyrene spheres across two-dimensional arrays of silicon cantilevers. On the surface of the single-crystal silicon resides a less than 2-nm-thick native silicon dioxide layer along with various defect sites related to oxygen vacancies.[31,32] Because the polystyrene spheres are negatively charged, they are electrostatically attracted to the slight positively fixed charge

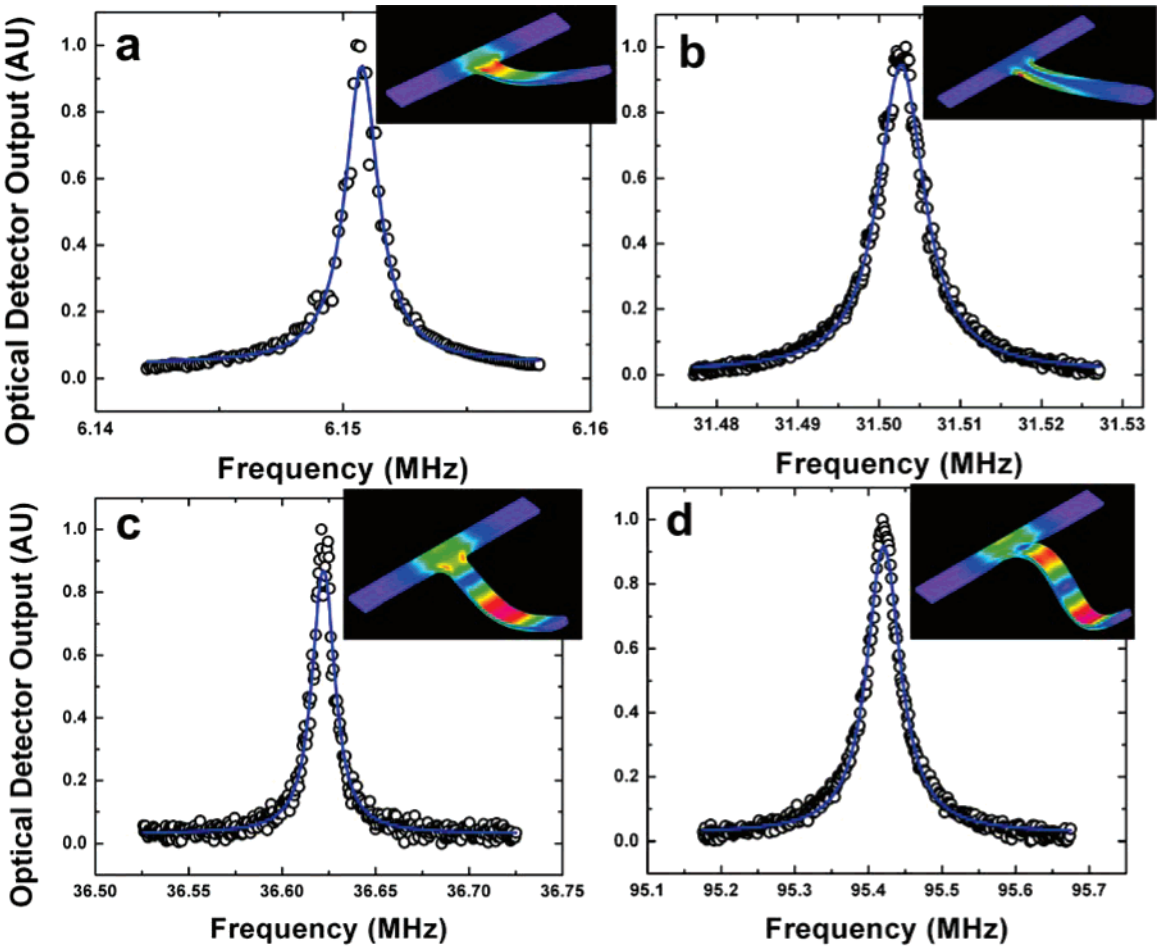

Figure 2. Measured frequency spectra (open circles) of a Si NEMS oscillator corresponding to various modes of vibration. The solid curve is a least-squares fit using a Lorentzian-type function. The insets represent the accompanying modes of vibration calculated using finite element analysis. Colors illustrate the effective modal stress of the first (a) transverse and (b) inplane and the (c) second and (d) third transverse modes. Because the in-plane mode shows the least amount of stress propagation into the overhang regime, the mechanical quality factor of this mode was highest.

Table 1. Calculated and Measured Eigenfrequency and Mechanical Quality Factor (Q) of Various Modes for a 6.6-μm-Long, 1-μm-Wide, and 200-nm-Thick Cantilever

ξ	mode type	beam theory (MHz)	FE (MHz)	experimental results (MHz)	Q
1	out-of-plane I	6.36	5.91	6.15	3425
2	in-plane I	31.79	32.20	31.50	4736
3	out-of-plane II	39.84	35.76	36.62	2745
5	out-of-plane III	111.54	95.83	95.42	1807

states residing at the native oxide surface. Chemical bonds and capillary forces due to monolayers of water present in the ambient environment are possible additional mechanisms of colloidal adhesion to the oscillator surface.

Oscillators containing single latex spheres were then identified using scanning electron microscopy (Figure 3b and c) and placed into a chamber that was evacuated to a pressure of 2×10^{-7} Torr. NEMS devices with single latex spheres were baseline-measured using a low excitation signal. The incident HeNe laser power was 56.4 μW during the baseline measurements. To maximize the in-plane vibrations, we placed the excitation source asymmetrically in such a way that the laser spot was offset to one side of the cantilever near the clamped end. The induced thermal gradient across the width of the beam gives rise to amplified in-plane vibrations.[33,34]

Figure 4a shows the in-plane spectra of the first vibrational mode with the sphere and following the removal of the sphere by shaking. Figure 4b shows the measured resonant transverse harmonic before and after the removal of the polystyrene sphere. Here the oscillator had the following dimensions: $w = 601$ nm, $l = 10.12$ μm, and $t = 250$ nm. Figure 4c and d show oblique angle scanning electron micrographs of the cantilever with a polystyrene sphere near the free end and directly following the removal of the bead, respectively. We found that even at extreme driving amplitudes where the NEMS is impacting the substrate out-of-plane excitations were insufficient for removing bound polystyrene particles. Baseline measurements on a collection of oscillators with these dimensions had a natural out-of-plane harmonic of 3.16 ± 0.12 MHz. This was in excellent agreement with the results following the removal of the sphere. Polystyrene removal experiments were carried out on more than 20 oscillators with dimensions ranging from $l = 6-12$ μm, $w = 500$ nm-1 μm, and $t = 200$ and 250 nm.

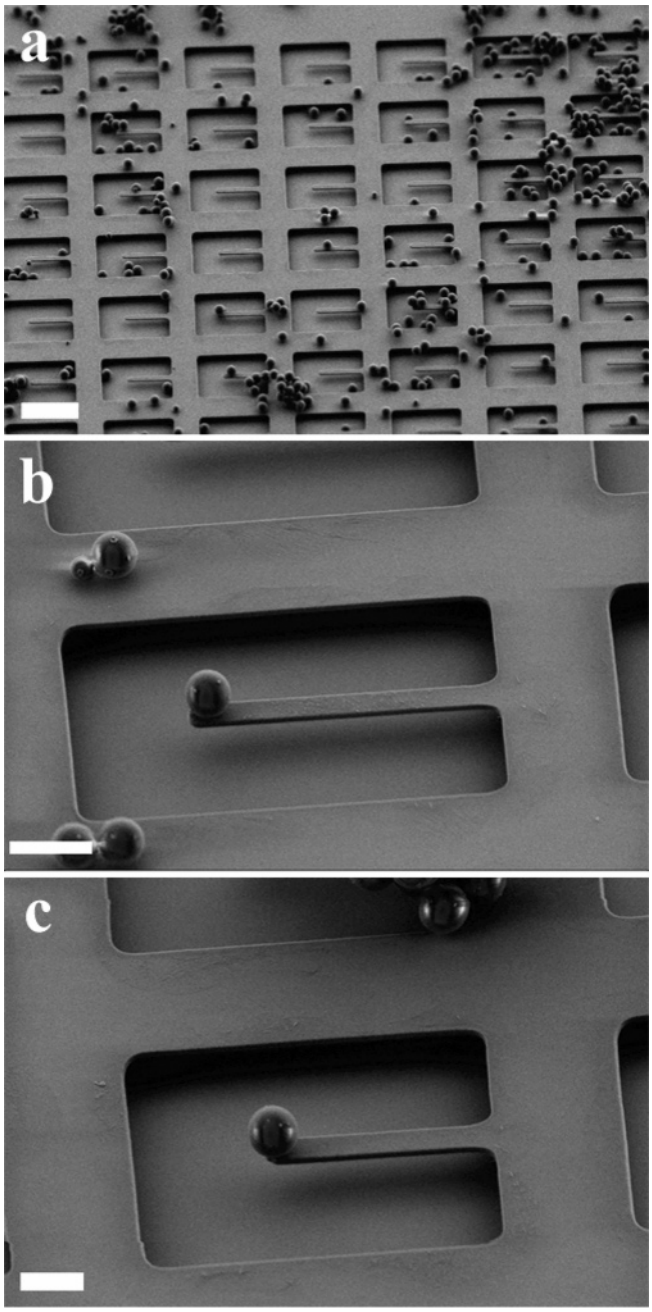

Figure 3. Oblique angle scanning electron micrographs of (a) arrays of 250-nm-thick single-crystal silicon suspended cantilever devices with attached polystyrene spheres. The scale bar corresponds to 10 μm. Single polystyrene spheres near the free end of the released structures with dimensions of $w = 1$ μm, (b) $l = 10$ μm, and (c) $l = 6.5$ μm. The scale bar corresponds to (b) 3 μm and (c) 2 μm.

For comparison to other methods of force generation, the magnitude of the force required for detachment was much greater than that achieved by rotating the sample on a conventional photoresist spinner. For example, we identified the positions of various spheres at distances ranging from 500 μm to 4 mm away from the axis of rotation and spun the sample at rotational frequency of 5 krpm. This did not generate enough force to remove any of the identified spheres from the surface.

The detachment mechanism could be described qualitatively as a peeling due to rolling of the sphere along the oscillator under an inertial force. This force, reduced to a shear force at the interface between the sphere and the beam, is responsible for sliding of the sphere as well as for the moment that leads to rolling of the sphere. Considering harmonic oscillations, the amplitude of the inertial force is $F_i = (2\pi f)^2\ b(4/3)\ \pi r^3 \rho$ where f is the frequency, b is the vibrational amplitude at the attachment point, and r and ρ are the radius and density of the polystyrene sphere, respectively. The ratio between the in-plane and out-of-plane forces is $F_i/F_o = (f_i^2 b_i)/(f_o^2 b_o) = (w^2 b_i)/(t^2 b_o)$ and is relatively large for $w > t$ and $b_i \approx b_o$ because of a higher in-plane resonant frequency. Assuming equal amplitudes of the out-of plane and in-plane vibrations, $b = 250$ nm, the experimentally measured values of f (given in Table 1), $r = 250$ nm and $\rho = 1000$ kg/m^3; the inertial forces are 25.8 and 679.4 nN for the first out-of-plane and in-plane modes, respectively.

Because of the interactions between the polystyrene spheres and the Si oscillator, at the interface finite contact area, a, exists[35] (see Figure 5). To compare detachment in the normal direction and the force required to initialize rolling, we consider out-of-plane vibration wherein the detachment force acting in the direction perpendicular to the beam surface is obtained as a value at which the radius a of the contact area shrinks to zero $F_{\mathrm{OUT}}^{\mathrm{MAX}} = (3/2)\gamma\pi r$.[35] Here γ is the free surface energy. In the case of in-plane vibration, under the assumption that the peeling surface energy, that is, the energy required to create new surfaces, is much higher than the energy released when two surfaces are attached to each other,[36] the force required to initiate rolling is $F_{\mathrm{IN}}^{\mathrm{MAX}} = \gamma\delta A/\delta u$.[36] Here, δu is the virtual displacement of the center of the sphere and $\delta A \sim 4a\delta u$ is the contact area change associated with δu (see Figure 5). Within this approach, the ratio between the detachment value of the out-of-plane and rolling value of the in-plane forces is $3\pi r/(8a)$. Because typically $r \gg a$, these results collectively provide compelling evidence that, in contrast to out-of plane vibrations, in-plane oscillations are a more-efficient mechanism for detachment of bound particles.

In summary, we demonstrate the ability to actuate and observe in-plane oscillations of cantilever beams using optical excitation and interferrometric detection. These modes of vibration were not observed with kinematic actuation when the devices were attached to a vibrating piezoelectric transducer.[37] Furthermore, these vibrational modes were used for nanomanipulation of submicrometer spherical particles. The complex dynamics of the in-plane vibrational effects of loosely bound particles on the surface of nanomechanical resonators could be exploited for implementing coherent control of functionalized oscillators in biosensing applications. In a fluid environment for instance, in-plane vibrations induced by the resonator would give rise to shear forces acting on the surface of the resonator. A related natural extension of this process concerns the ability to distinctly engineer nanoscopic surface properties of individual elements in large NEMS arrays. Consequently, excitations generating drag forces on the surface of NEMS associated with this methodology would be optimized to a regime where chemi-

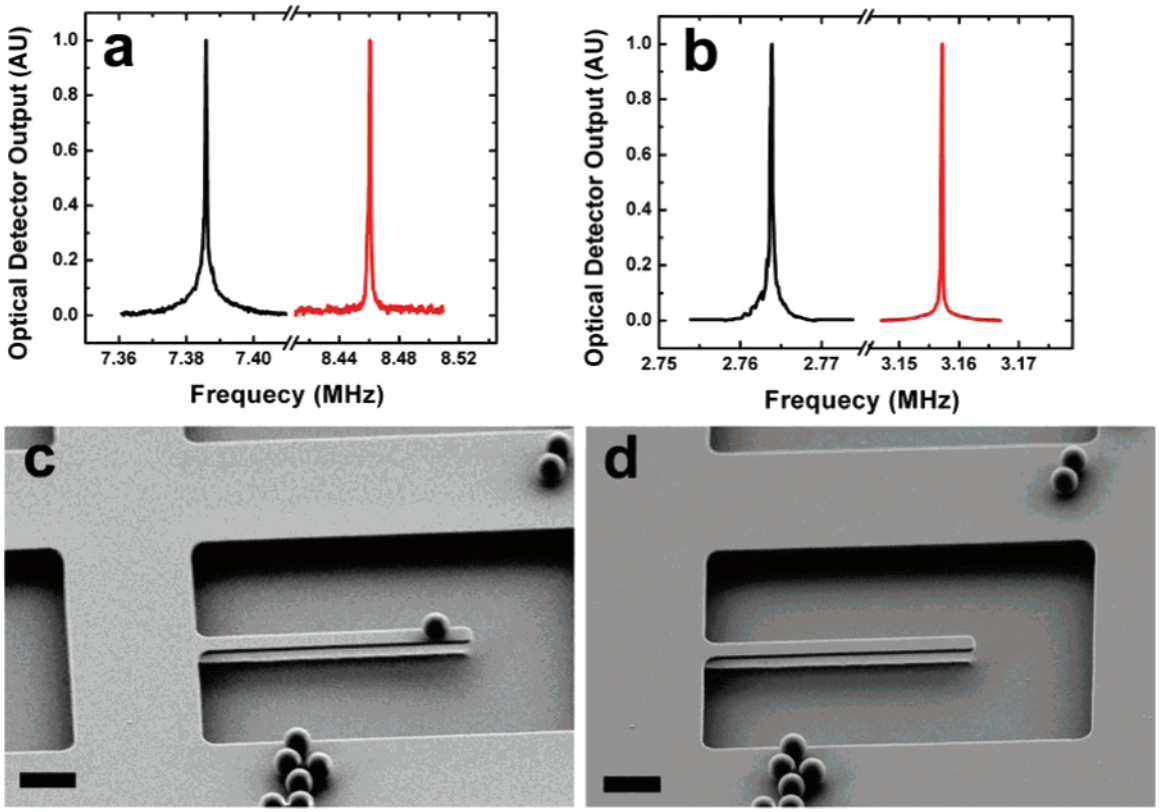

Figure 4. Measured frequency spectra before (black) and after (red) the detachment of the polystyrene sphere for the (a) in-plane and (b) transverse vibrational modes. Oblique angle scanning electron micrographs (c) before and (d) after the polystyrene sphere detachment from the surface of the corresponding NEMS device with dimensions of $w = 601$ nm, $l = 10.12$ μm, and $t = 250$ nm. The scale bar represents 2 μm.

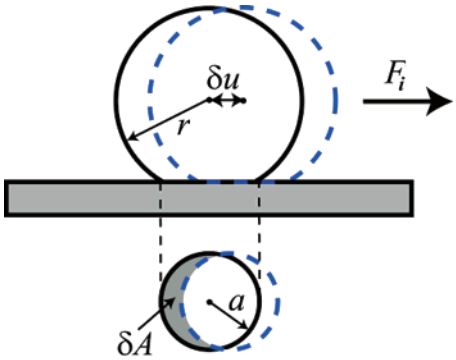

Figure 5. The cross-sectional schematic (top image) illustrates the dynamic mechanism of the spherical particle detachment from the surface of the silicon oscillator an inertia force F_i. The dashed blue line highlights the new position of the sphere resulting from the initiation of rolling due to F_i. The bottom image represents a projection along the oscillator surface, illustrating that the radius of the sphere contact area, a, and the crescent-shaped released area, δA, are associated with the virtual displacement, δu, of the center of the sphere.

sorbed, selectively bound molecules are unaltered, while weakly attached species are removed across arrays of oscillators. This provides an alternative mechanism for minimization of nonspecifically bound molecules in sensing applications. This inevitable continuation toward more complex devices further leads to a proliferation of novel NEMS devices with highly useful characteristics. A satisfactory theoretical treatment of nonlinear wave propagation in conjunction with fluid structure interaction should lead to a wide wealth of shear wave propagation phenomenon along the surface of the NEMS oscillator.

Acknowledgment. We thank R. Lovelace, M. Guillorn, F. Rizzo, C. Burger, S. Verbridge, and B. Cipriany for helpful suggestions and discussions, and the staff at the Cornell Nanoscale Facility for generous aid in fabrication. This work was supported by DARPA, NSF through the Nanobiotechnology Center, and New York State.

References

(1) Newell, W. E. *Science* **1964**, *161*, 1320.
(2) Petersen, K. E. *IEEE Trans. Electron Devices* **1978**, *25*, 1241.
(3) Petersen, K. E. *Proc. IEEE* **1982**, *70*, 420.
(4) Turner, K. L.; et al. *Nature* **1998**, *396*, 149.
(5) Grade, J. D.; Jerman, H.; Kenny, T. W. *J. Microelectromech. Syst.* **2003**, *12*, 335.
(6) Riehl, P. S.; Scott, K. L.; Muller, R. S.; Howe, R. T.; Yasaitis, J. A. *J. Microelectromech. Syst.* **2003**, *12*, 577.
(7) Dohn, S.; Sandberg, R.; Svendsen, W.; Boisen, A. *Appl. Phys. Lett.* **2005**, *86*, 233501.
(8) Sato, M.; Hubbard, B. E.; Sievers, A. J. *Rev. Mod. Phys.* **2006**, *78*, 137.
(9) Sadewasser, S.; Villanueva, G.; Plazaa, J. A. *Appl. Phys. Lett.* **2006**, *89*, 033106.
(10) Carr, D. W.; Craighead, H. G. *J. Vac. Sci. Technol., B* **1997**, *15*, 2760.
(11) Carr, D. W.; Evoy, S.; Sekaric, L.; Craighead, H. G.; Parpia, J. M. *Appl. Phys. Lett.* **2000**, *77*, 1545.
(12) Craighead, H. G. *Science* **2000**, *290*, 1532.
(13) Schwab, K. *Appl. Phys. Lett.* **2002**, *80*, 1276.
(14) Knobel, R. G.; Cleland, A. N. *Nature* **2003**, *424*, 291.

(15) Cleland, A. N.; Geller, M. R. *Phys. Rev. Lett.* **2004**, *93*, 070501.
(16) Aldridge, J. S.; Cleland, A. N. *Phys. Rev. Lett.* **2005**, *94*, 156403.
(17) Fennimore, A. M.; et al. *Nature* **2003**, *424*, 408.
(18) Sazonova, V.; et al. *Nature* **2004**, *431*, 284.
(19) Papadakis, S. J.; et al. *Phys. Rev. Lett.* **2004**, *93*, 146101.
(20) Bourlon, B.; Glattli, D. C.; Miko, C.; Forro, L.; Bachtold, A. *Nano Lett.* **2004**, *4*, 709.
(21) Meyer, J. C.; Paillet, M.; Roth, S. *Science* **2005**, *309*, 1539.
(22) Williams, P. A.; et al. *Appl. Phys. Lett.* **2003**, *82*, 805.
(23) Meyer, G.; Amer, N. M. *Appl. Phys. Lett.* **1988**, *53*, 2400.
(24) Sarid, D. *Scanning Force Microscopy with Applications to Electric, Magnetic and Atomic Forces*; Oxford University Press: London, U.K. 1991.
(25) Zalalutdinov, M. *Appl. Phys. Lett.* **2001**, *78*, 3142.
(26) Ilic, B.; Krylov, S.; Aubin, K.; Reichenbach, R.; Craighead, H. G. *Appl. Phys. Lett.* **2005**, *86*, 193114.
(27) Ilic, B.; Yang, Y.; Aubin, K.; Reichenbach, R.; Krylov, S.; Craighead, H. G. *Nano Lett.* **2005**, *5*, 925.
(28) Timoshenko, S.; Young, D. H.;Weaver, W. *Vibration Problems in Engineering*; Wiley: New York, 1974.
(29) Sato, M.; et al. *Phys. Rev. Lett.* **2003**, *90*, 044102.
(30) Kesavamoorthy, R.; Sakuntala, T.; Arora, A. K. *Meas. Sci. Technol.* **1990**, *1*, 440.
(31) Schroder, D. K. *Semiconductor Material and Device Characterization*; Wiley-Interscience: New York, 1998.
(32) Laws, G. M.; et al. *Physica E* **2003**, *17*, 659.
(33) Lammerink, T. S. J.; Elwenspoek, M.; Fluitman, J. H. J. *Proc. IEEE Micro Electro Mech. Syst., MEMS '91*, **1991**, 160.
(34) Mahameed, R.; Elata, D. *J. Micromech. Microeng.* **2005**, *15*, 1414.
(35) Johnson, K. L.; Kendall, K.; Roberts, A. D. *Proc. R. Soc. London, Ser. A* **1971**, *324*, 301.
(36) Roberts, A. D. *J. Phys D: Appl. Phys.* **1977**, *10*, 1801.
(37) Ilic, B.; Craighead, H. G.; Krylov, S.; Senaratne, W.; Ober, C.; Neuzil, P. *J. Appl. Phys.* **2004**, *95*, 3694.

NL0621950